ANTIPYRINE REMOVAL BY TiO_2 PHOTOCATALYSIS BASED ON SPINNING DISC REACTOR TECHNOLOGY

A.J. Expósito[1], D.A. Patterson*[2], W.S.W. Mansor[2], J.M. Monteagudo[1], E. Emanuelsson[2], I. Sanmartín[1], A. Durán*[1]

[1] Department of Chemical Engineering, Grupo IMAES. Escuela Técnica Superior de Ingenieros Industriales, Instituto de Investigaciones Energéticas y Aplicaciones Industriales (INEI) Universidad de Castilla-La Mancha, Avda. Camilo José Cela 3, 13071 Ciudad Real (Spain). Phone: 0034 926295300, ext: 96565. email: antoniojose.exposito@uclm.es

[2]Bath Process Intensification Laboratory and Centre for Advanced Separations Engineering, Department of Chemical Engineering, University of Bath, BA2 7AY, UK.

* To whom correspondence should be addressed

ABSTRACT

The photo-degradation of the emerging contaminant antipyrine (AP) was studied and optimized in a novel photocatalytic spinning disc reactor (SDR). A heterogeneous process ($UV/H_2O_2/TiO_2$) was used. TiO_2 was immobilized on the surface of a glass disc using a sol-gel method. A factorial design of experiments followed by a Neural Networks fitting allowed the optimal conditions to be determined for treating 50 mg/L of AP. Under these conditions (pH= 4; $[H_2O_2]_0$= 1500 mg/L; disc speed= 500 rpm; flowrate = 25 mL/s), AP was completely degraded in 120 minutes and regeneration of the disc allowed 10 cycles with no loss in efficiency. The value of the apparent volumetric rate constant was found to be $6.9 \bullet 10^{-4}$ s^{-1} with no apparent mass transfer limitation.

Based on the main intermediates identified, a mechanism is proposed for antipyrine photodegradation: Firstly, cleavage of the N-N bond of penta-heterocycle leads to the formation of two aromatic acids and N-phenylpropanamide. An attack to the C-N bond in the latter compound produces benzenamine. Finally, the phenyl ring of the aromatic intermediates are opened and molecular organic acids are formed.

* corresponding authors: email: antonio.duran@uclm.es; d.patterson@bath.ac.uk

Keywords: AOPs; emerging contaminant; neural netwoks; pathway; pharmaceuticals; UV radiation

1. INTRODUCTION

Emerging contaminants (EC) have received significant attention in the recent years since they are new chemicals whose effects are unknown on environment and human health (Durán et al., 2013). Therefore, EC are shown as potential pollutants which must be removed. Antipyrine (AP), which is included in this group, is a common analgesic and anti-inflammatory drug used ubiquitously by the pharmaceutical industry. AP is a complex molecule which is not able to be removed by the traditional techniques used in wastewater treatment, hence it can be accumulated in the natural water cycle (Verlichi et al., 2012). At present, low concentrations of antipyrine have been measured in previous works at up to the μg/L level in municipal sewage effluents, ground water and drinking water (Cai et al., 2013).

Advanced Oxidation Processes (AOPs) have been shown to be a potential technique that is able to remove refractory molecules. These processes are based on the production of highly reactive radicals Liu et al., 2016). The radicals have a short life, reacting quickly and can mineralize the organic pollutants. One of the most interesting AOPs consists of the use of semiconductors as photocatalysts. The semiconductor TiO_2 has been extensively studied because of its high photo-reactivity, stability to corrosion/dissolution, low price, ready availability and ability to generate electron-hole pairs when illuminated by UV which initiate both radical generation and direct oxidation of organic pollutant species, enabling mineralization to be achieved (Naeem and Ouyang, 2013; Domínguez et al., 2015). In addition, it is not toxic, it is biologicallly and chemically inert and it can be regenerated several times without significant loss of activity. However, comparing TiO_2 results between different scales and configurations is difficult, complicating its

applicability (Rao and Chu, 2009; Domínguez et al., 2015). This is in the main due to the almost universal application of TiO_2 as a powder suspension, which when applied in different reactor systems and at different scales produces a difficult to predict change in photo-reactivity due to complex to model effects such as light scattering, shadowing, mass transfer limitations in multiphase flow systems (such as is the norm in gas-liquid-solid or liquid-solid photocatalytic systems). Recovery of the suspended catalyst can also complicate and increase the cost of the overall process, which may be a further barrier to implementation and comparison between different configurations. Consequently, using immobilised/supported TiO_2 is a simple way to overcome most, if not all, of these problems, in particular enabling simpler scale-up since there is no solid phase creating multiphase flow, shadowing and avoiding the need for photocatalyst separation (Boiarkina et al., 2011). Sol-gel coating is an established method for the synthesis of thin and porous layers of TiO_2 and as such is used in this work (Miranda-García et al., 2014).

The use and properties of H_2O_2 as an oxidant is thoroughly known. It can be easily activated by UV light generating hydroxyl radicals. Furthermore, H_2O_2 is cheap, easily stored and it is soluble in water, with negligible mass transfer limitations (Li et al., 2015). There are several studies which have shown the improvement of TiO_2 effectiveness in the presence of H_2O_2 because it can react with TiO_2 giving rise to the formation of Ti-OOH complexes (Li et al., 2001; Domínguez-Sanchez et al., 2013). This complex has a coloured surface which enhances the photocatalyst effect Li et al., 2001).

Despite all of the extensive work on photocatalysis and processes based on TiO_2 they still suffer from particularly show slow kinetics and low mass transfer. It is therefore necessary to find new ways able to improve the efficiency. Intensification processes can

115 reduce costs, increase the intrinsic safety and minimize the environmental impact, as well
116 as enhance the efficiency (Ling et al., 2004). The Spinning Disc Reactor (SDR) is an
117 intensification process based on the creation of a thin film. The reactor consists of a
118 spinning disc, where the feed fluid is fed to the centre top surface of the disc. In the
119 photocatalytic SDR, the surface of the disc is coated with the photocatalyst. The feed fluid
120 is spread out over the surface of the disc because of the centrifugal acceleration,
121 generating a thin film of 20-200 μm (Boodhoo et al., 2000). The thin film improves the
122 mass and heat transfer, especially in solid-liquid systems, and the penetration of UV light
123 to the surface of the disc, which can be an advantage over other types of photoreactor
124 systems when using coloured and/or UV light absorbing solutions, since this facilitates
125 higher light penetration to the photocatalyst per volume of feed on the catalyst, increasing
126 the volumetric efficiency of the reaction. Moreover, shorter retention times are needed
127 since the efficiency is increased. Boiarkina et al. (2011) verified that the effect of the flow
128 and the speed of the disc were important in this kind of reactor because these two
129 parameters have a significant influence on the flow regime and therefore in the mass and
130 heat transfer to and from the photocatalyst surface.
131 The behaviour of the photocatalytic SDR for pollutant removal has been studied for
132 methylene blue (Ling et al., 2004; Boiarkina et al., 2011; Boiarkina et al., 2013) as a
133 common reference pollutant and dehydroabietic acid (Boiarkina et al., 2013), a pollutant
134 from the paper industry.
135 Therefore, the aim of this paper is to study the applicability of a TiO_2 photo-degradation
136 process to efficiently degrade a synthetic effluent containing antipyrine in a novel
137 spinning disc reactor (SDR). We are the first to comprehensively map out the effect of
138 the important operating parameters of the photocatalytic spinning disc reactor, by
139 applying statistical experimental design. As this has not been done for SDRs in general,

this paper is the first comprehensive assessment of the operating space for this important class of process intensification reactor. To this end, a factorial design of experiments which is a proven technique successfully used in removal of pollutants with AOPs (Monteagudo et al., 2008) was used changing four variables. Later, experimental results of antipyrine degradation were fitted with neural networks (NNs) since they have shown to be robust and applicable in almost all situations (Khatae and Kasiri, 2010). In addition, by analysis of reaction products by high performance liquid chromatography (HPLC) and liquid chromatography-mass spectroscopy (LC-MS), this paper proposes a new and comprehensive photocatalytic degradation pathway for antipyrine.

2. EXPERIMENTAL

2.1. Materials

Antipyrine (99%) was obtained from Acros. 30% hydrogen peroxide (H_2O_2) and methanol (99.8%) were purchased from Fisher Scientific and VWR-Chemical respectively and were used as received. The pH of the solution was adjusted with H_2SO_4 and NaOH.

Acetic acid (99.7%, Sigma Aldrich), acetylacetone (99%, Sigma Aldrich) and isopropanol (99.5%, Sigma Aldrich) were used for sol-gel preparation. Deionized water used for preparing solutions was obtained from a purifying machine (ELGA PURELAB). Glass discs (200mm in diameter, 3mm thick) were supplied by Roman Glass (Bath, UK).

2.2. Experimental set-up and procedure

The experimental setup is shown in Figure 1. The experiments were carried out in recirculating batch mode. For the UV/H_2O_2/TiO_2 process, the solution to be treated (750 mL) is initially kept in a 1L reservoir under constant magnetic stirring. After pH fitting,

164 the solution is fed with a peristaltic pump (MasterFlex Easy-load II) into a tightly sealed
165 glass flask, which avoided the flow pulsations generated in the pumping process. Then
166 the solution is fed into the spinning disc reactor. Both the reservoir and the flask were
167 covered with aluminum foil in order to avoid the light incidence in case some TiO_2
168 particles were detached from the disc. The solution is cooled with tap water with a Liebig
169 cooler. The liquid containing AP goes into through the center of the disc where it falls
170 down on the disc spreading out the solution. During this process, the solution is irradiated
171 by a low pressure mercury UV lamp inside a quartz tube (20 W, monochromatic, λ=254
172 nm, Steriflow, supplied by Davey Water Products NZ, part nr. GPH369N/S). The lamp
173 is situated at the focus of a parabolic mirror in order to leverage the maximum possible
174 radiation. The liquid is collected by a funnel beneath the disc and is returned to the
175 reservoir by gravity.

176 The speed and flow were set for every experiment according to the experiment design as
177 explained below. The lamp was switched on and the H_2O_2 was added after 20 minutes in
178 the dark to allow pollutant adsorption by the TiO_2. Sodium sulfite anhydrous, Na_2SO_3
179 was used for quenching inmediatly after sampling. pH was kept constant (± 0.1) during
180 the experiments. In exceptional cases, addition of drops of sulfuric acid or sodium
181 hydroxide were needed.

182 Figure 1

183 **2.3. Analytical methods**

184 The removal of antipyrine was evaluated immediately after sampling using a Gilson 231
185 XL high performance liquid chromatography (HPLC) system with UV detection under
186 an isocratic mode and an Eclipse XDB-C18 column (5 μm, 4.6 × 250 mm). 60:40 (v/v)

methanol/(water with 0.1% acetic acid) mixture at acidic pH was used as the mobile phase (detection wavelength, λ= 252 nm; flow rate of 0.6 ml min^{-1}).

Total organic carbon concentration was determined using a TOC analyzer (Shimadzu TOC-5000A). H_2O_2 concentration was measured by titration with an aqueous solution of potassium permanganate (0.025 mol/L).

Intermediate by-products were identified by mass spectrometry (MS) using a TOF-MS micrOTOF-Q II (Bruker Daltonics Inc., Billerica, MA, USA) with electrospray ionization source and negative and positive-ion polarity equipped with a 2.5 mL or 500 µL Hamilton gastight syringe (Hamilton, Reno, NV, USA) to deliver the samples . MS measurements were taken over the range 50<m/z<600.

The X-ray diffraction spectrum obtained with a p-XRD-BRUKER D8-Advance (Cu radiation) shows characteristic anatase peaks. No rutile peaks are present.

2.4. Sol gel method for TiO_2 preparation

TiO_2 was supported onto the surface of the glass discs using a sol-gel process according to the method used by Boiarkina et al. (2013). The glass discs were extracted from the sol at 1 mm/s, allowed to air dry for 5 min in the fume-hood and then transferred to an oven at 100 ºC for 30 min. This process was repeated once more before the discs were transferred to a furnace (Gallenkamp Muffle Furnace Size 3 with a Vertex VT4826 controller) for calcination at 500 ºC for 1 hour to obtain the photocatalytically active anatase crystal structure. The furnace was ramped up at a rate of 2 ºC/min to minimize cracking. Once the discs had cooled, the process was repeated once more to obtain a total of four TiO_2 layers, two of which were calcined.

2.5. Factorial design and neural network strategy

A Central-Composite Experimental Design was applied to investigate the effects of four variables (initial concentration of hydrogen peroxide, speed of the disc, flowrate and pH) on the selected Response Function (degradation of antipyrine). It consisted of three series of experiments for k= 4 variables (Table 1) including:

i) a factorial design with 2k trials with all possible combinations of codified values +1 and –1), experiments 1 to 16 in Table 1

ii) selection of the axial distance of the star points (codified values $\alpha = 2k/4 = \pm 2$) consisting of 2k experiments 17 to 24 in Table 1, and

iii) replicates of the central point (four experiments, 25-28).

The complete experimental design and additional experiments, including variable ranges and the values of the obtained response functions, are also shown in Supplementary Material (Table 1). Disc speed and flow rate were changed into the allowed limits of the experimental set-up. pH was varied from 4 to 8 (above and below the the zero point charge for TiO_2, which is between 5.6 and 6.4). Lower pHs were not tested, since the mirrored chrome UV-lamp protection in the reactor could be damaged.

Supplementary material, Table 1

The experimental results (removal of AP in each test) were fitted using a neural network applied with two neurons, previously used in literature (Monteagudo et al., 2008). It uses a simple exponential activation function and a solution strategy based on a back-propagation algorithm (Morgan and Scofield, 1991). Parameters were fitted using the Solver tool in a custom spreadsheet in Microsoft Excel using a nonlinear fitting method. As a final point, a measure of the saliency of the input variables was made to analyze the relevance of each variable with respect to the others (expressed as percentages) based on the connection weights of the neural networks (Nath et al., 1997). Fitting with a

polynomial model derived from the factorial design was also tested, but error estimation was higher, so it was discarded.

3. RESULTS AND DISCUSSION

3.1. Synergic effect

Firstly, some control and initial experiments were carried out to analyze the viability of this novel reactor technology for AP photocatalytic degradation. These experiments were run under the following conditions: speed = 300 rpm; flowrate = 25 mL/s; TiO_2 = 0.4 g; [H_2O_2] = 1000 mg/L. The results obtained are shown in Figure 2.

Figure 2

It can be seen that TiO_2 alone does not degrade AP at all. Molecular degradation with H_2O_2 reaches up to about 12.6 % of AP degradation, whereas UV photo-degradation produces up to 76.4 % of AP removal in 120 minutes. UV/H_2O_2 and UV/H_2O_2/TiO_2 processes reach 93% and 95.9% respectively, although the overall process is faster at the beginning. The increase in the kinetic constant is 6% if we consider the whole operating time. In addition, a low synergic effect can be seen among these processes during the first 40 minutes of reaction. For this reason, this system was selected for the experimental design.

The synergism between the individual processes and the overall UV/H_2O_2/TiO_2 system was quantified using the first order rate constants for AP removal according to equation (1) (Joseph et al., 2011):

$$Synergy\ (\%) = \frac{k_{UV/H2O2/TiO2} - (k_{UV/H2O2} - k_{UV/TiO2})}{k_{UV/H2O2/TiO2}} = \frac{0.0403 - (0.0223 + 0.0163)}{0.0403} = 4.21 \quad (1)$$

The detailed mechanism of this process has been widely discussed in the literature for different pollutants (Galindo et al., 2001; Daneshvar et al., 2004). The high oxidative

potential of the hole (h_{VB}^{+}) photogenerated in the catalyst allows the direct oxidation of the organic molecule (AP) to reactive intermediates. Hydroxyl radicals, HO•, are produced from H_2O_2 photodecomposition, but can also be formed either by the oxidation of water or by the reaction of the hole with OH^-. The photogenerated electrons in the conduction band (e_{CB}^{-}) on the catalyst surface can reduce molecular oxygen, adsorbed on the TiO_2 surface or dissolved in water, to superoxide anion or reduce the pollutant molecule. ·OH radicals together with other oxidant species such as peroxide radicals are thus responsible for the heterogeneous TiO_2 photodecomposition of AP.

3.2. Effect of variables

A complete set of experiments were made based on the previously described factorial design to analyze the effect of four parameters (speed of the disc, flowrate, pH and initial concentration of hydrogen peroxide). The initial antipyrine concentration was 50 mg/L. However, after analyzing the results, two additional experiments increasing the concentration of H_2O_2 were made in order to obtain the optimal conditions. The complete series of tests is shown in Table 1 together with AP removal after 120 minutes.

The experimental results obtained for AP degradation were fitted with NNs, resulting in an average error of less than 4% (Supplementary material, Figure S1). The equation and fitting parameters are shown Supplementary material (Table 2). N_1 and N_2 are general factors related to the first and the second neurons, respectively. W_{11} to W_{14} are the contribution parameters to the first neuron and represent the influence of each of the variables in the process (initial concentration of H_2O_2, disc speed, flow and pH); W_{21} to W_{24} are the contributions to the second neuron corresponding to the same variables.

Supplementary material (Table 2, Figure S1)

The results of saliency analysis on the input variables for each neural network (%) are shown in Supplementary material (Figure S2). From these results, it was possible to

284 deduce the effect of each parameter on the antipyrine removal. Thus, it was confirmed
285 that the removal was mainly influenced by the initial concentration of hydrogen peroxide
286 (69.5%).

287 Supplementary material (Figure S2)

288 A simulation of the influence of each parameter from NNs equation is shown in Figure 3.
289 A decrease in pH slightly improves AP degradation (Figure 3a). The differences in
290 photoactivity of various substrates at different pHs are mainly attributable to the different
291 equilibrium species present in solution. It is not easy to correlate the photoreactivity with
292 the properties of molecules, but an attempt can be made by considering their pK_a values.
293 The zero point charge for TiO_2 is at pHs between 5.6 and 6.4 (Monteagudo et al., 2008).
294 Hence, at more acidic pH values, the TiO_2 surface is positively charged. The slight
295 increase in degradation efficiency in our case can be explained by considering that only
296 one main species for AP is likely to exist at the different pHs tested (from 4 to 8), owing
297 to the AP pK_a being 1.4 (Molinari et al., 2006). Considering that a low pH could damage
298 the mirrored chrome UV-lamp protection in the reactor, pH=4 was consequently selected
299 as the optimal value.

300 Figure 3

301 The optimal initial concentration of H_2O_2 was found to be around 1500 mg/L (Figure 3a).
302 The excess of H_2O_2 reacts with the HO• radicals to produce HO_2• radicals, which are less
303 reactive, decreasing AP degradation according to the well-known scavenger effect:

304 $$H_2O_2 + HO\cdot \rightarrow HO_2\cdot + H_2O \quad (2)$$

305 Additionally unproductive reactions may also occur:

306 $$HO\cdot + HO\cdot \rightarrow H_2O_2 \quad (3)$$

307 $$HO\cdot + HO_2\cdot \rightarrow H_2O + O_2 \quad (4)$$

308

309 Finally, it is also evident from Figure 3b that the disc speed and the flowrate favor a mass
310 transfer rate producing a higher AP degradation. For disc speed, an additional effect is
311 the increased mass transfer of oxygen into the system through the air-water interface on
312 the liquid film surface of the spinning disc. This dissolved oxygen has the potential to be
313 an additional oxidant source, potentially enhancing degradation rate. The maximum
314 allowed values of these parameters were consequently selected as optimal conditions
315 (speed = 500 rpm; flowrate = 25 mL/s).
316 Previous works with SDR treating methylene blue (Boiarkina et al., 2011) concluded that
317 mass transport limitations were affecting the reaction rate, since they did not find any
318 correlation between the photonic efficiency with the film height. The authors
319 recommended to increase mixing and turbulence on the disc in future works in order to
320 eliminate the mass transfer perpetrated reaction rate drop.
321 In order to determine if mass transfer limitation is occurring in our system, the film height
322 distribution across the surface has been calculated using the Nusselt model that assumes
323 laminar flow across the surface of the disc according to Eq (5) (Burns et al., 2003).

324 $$h = \left(\frac{3Q\upsilon}{2\pi r^2\omega^2}\right)^{1/3} = Ar^{-2/3} \quad (5)$$

325

326 Where h is the liquid film thickness at radius r, Q is the volumetric flow rate, υ is the
327 kinematic viscosity, ω is the rotational speed and A is a parameter combining all the
328 constants.

329

330 This model can be used as an approximation for Ekman numbers higher than 2 (Burns et
331 al., 2011) or 1.62 (Caprariis et al., 2012). However it can not be used accurately for the
332 inertial flow conditions characterized by low Ekman numbers, which is defined in
333 equation (6) as:

$$E = \left(\frac{\nu}{h^2\omega}\right) \qquad (6)$$

In this work, the Ekman number range was between 0.1 and 6.9, being higher than 2 for r/R> 0.33. This means that there will be some error in thin film estimation near the center of the disk. In spite of this limitation, average results for thin film height for all the tests are shown in Table 1. Figure 4 shows the film height distribution for optimal conditions.

Figure 4

On the other hand, assuming a pseudo-first order reaction $R_i = -kC$, with k being a pseudo-constant including the contribution of both the kinetic constant and the concentration of hydrogen peroxide (which would be in great excess) and considering that the SDR behaves like a plug flow reactor (Boiarkina et al., 2011), leads to the following expression for the change in concentration with respect to radius:

$$C = C_0 exp\left(\frac{Q}{V}\left[exp\left(-\frac{3\pi Ak}{2Q}\left(R^{4/3} - {R_0}^{4/3}\right)\right) - 1\right]t\right) \qquad (7)$$

where R is the outer radius of the disc and R_0 is the inlet nozzle radius. A plot of ln (C/C_0) versus time should yield a straight line relationship for a pseudo-first order reaction (see figure S3 in supplementary material).

Figure S3

Although the model is just an approximation, there is no apparent decrease in the order of magnitude of reaction rate (the apparent volumetric rate constant ranges from $2.05 \bullet 10^{-4}$ to $4.82 \bullet 10^{-4}$ s^{-1} as summarized in Table 1) with film height (111-222 μm). Additionaly, the irradiance profile is relatively uniform due to the parabolic mirror with the UV lamp in its focus. There is no dependence of the photonic efficiency on the film height, since the irradiance profile varies from 12 to 23 W/m^2, in the same order of

358 magnitude (Boiarkina et al, 2011). Consequently, it is reasonable to believe that no mass
359 transfer limitations are occurring.

360

361 **3.3. Optimal conditions selected**

362 The degradation of AP and the evolution of the concentration of H_2O_2 under optimal
363 conditions are shown in Figure 5a. Under these conditions (pH= 4; $[H_2O_2]_0$= 1500 mg/L;
364 Speed= 500 rpm; Flow= 25 mL/s; $[AP]_0$= 50 mg/L), AP was completely degraded after
365 120 minutes. H_2O_2 still remained in solution, so that degradation of intermediate products
366 could be achieved. However, as shown in Figure 5b, mineralization is very slow, reaching
367 only 35% in 4 hours.

368 Figure 5

369 New experiments were conducted increasing temperature up to 45 and 60 ºC under
370 optimal conditions to try to improve reaction kinetics (Figure 6). However, no positive
371 effect was obtained since dissolved oxygen (DO) is lower when increasing temperature,
372 and accordingly a lower concentration of radicals are formed according to the main
373 reactions involved when H_2O_2 and O_2 are present in solution (Miralles-Cuevas et al.,
374 2014):

375 $$R + HO\cdot \rightarrow R\cdot \quad (8)$$

376 $$R\cdot + O_2 \rightarrow ROO\cdot \quad (9)$$

377 $$ROO\cdot + RH \rightarrow ROOH + R\cdot \quad (10)$$

378 $$ROO\cdot + H_2O \rightarrow ROH + HO_2\cdot \quad (11)$$

379 $$HO_2\cdot + H_2O_2 \rightarrow HO\cdot + H_2O + O_2 \quad (12)$$

380 $$HO\cdot + H_2O_2 \rightarrow HO_2\cdot + H_2O \quad (13)$$

381

382 Furthermore, H_2O_2 is decomposed by unproductive reactions at high temperatures.

383 Figure 6

384

385 In order to confirm that hydroxyl radical is the main active species responsible for the
386 degradation of antipyrine in this system, comparison experiments of scavenger-loaded
387 conditions with 200 mM methanol (an hydroxyl radical scavenger, $k = 9.7\times10^8$ $M^{-1}s^{-1}$)
388 were undertaken (Matta et al., 2011). It can be seen that methanol slows the antipyrine
389 degradation rate (Figure S4). Total inhibition is not achieved due to UV radiation and in
390 a lower extent to molecular degradation with H_2O_2 (see Figure 1).

391 Figure S4

392 **3.4. Intermediates and proposed pathway**

393 Intermediates/by-products were identified using a mass spectrophotometer (Figure 7).
394 Although it is a qualitative analysis, the main intermediates could be identified and were
395 observed in the system to be benzenamine, anthranilic acid and butanedioic acid. Their
396 concentration increased until 1 hour of reaction, and decreased slowly later, indicating
397 that they are very difficult to mineralize using the UV/H_2O_2/TiO_2 system in the SDR.
398 Other intermediates found in minor concentration were fumaric acid, 4-oxo-pentanoic
399 acid, 1,4 benzenedicarboxylic acid and N-phenyl propinamide.

400 Figure 7

401 The toxicity of some intermediates, especially benzenamide (which is the main
402 constituent) is higher than antipyrine (Miao et al., 2015), so its mineralization is extremely
403 important.

404 The knowledge on the degradation products of AP during UV-based AOPs is highly
405 limited (Tana et al., 2013). According to literature, degradation of AP with different AOPs
406 may proceed with different intermediates. Tana et al. (2013) also identified N-
407 phenylpropinamide and benzenamine in the UV/H_2O_2 treatment process, while only N-

408 phenylpropinamide was detected in the UV/persulfate system. They proposed a
409 degradation pathway based on the attack of C-C bond in the pentacyclic ring by HO•
410 leading to the formation of N-phenylpropinamide. Subsequently, hydroxyl radicals
411 continued to attack the C-N bond in branch to produce benzenamine.

412 In contrast, in the UV/persulfate system, sulfate radicals seemed not to decompose N-
413 phenylpropinamide into benzenamine, so that degradation would progress in a different
414 pathway.

415 In our case, the high concentration of benzenamide and low concentration of N-
416 phenylpropinamide found seems to indicate that the UV/H_2O_2/TiO_2 process degradation
417 mechanism is similar to that occurring in the UV/H_2O_2 system.

418 The main intermediates found in this research also included small concentrations of
419 aliphatic acids (1,4-benzenedicarboxylic acid, 4-oxo-pentanoic acid and 2-butenedioic
420 acid) which agrees with previous findings found for AP degradation in a UV/H_2O_2/Fe/US
421 system (Durán et al., 2013). Thus, an adapted mechanism can be propsed for AP
422 photodegradation in Figure 8 for the UV/H_2O_2/TiO_2 process. The cleavage of the N-N
423 bond of penta-heterocycle leads to the formation of two aromatic acids and N-
424 phenylpropanamide. An attack to the C-N bond in the latter would produce benzenamine.
425 Finally, the phenyl ring of all of them is opened and small molecular organic acids are
426 formed. In a later stage, these acids may decompose into CO_2.

427 Figure 8

428 Given the above mechanism and the previous results, this work shows that the
429 phocatalytic SDR is an effective and robust wastewater treatment technology for the
430 degradation of antipyrine producing degradation products (such as molecular organic

acids) that could be further mineralised by conventional biological wastewater treatment systems.

3.5. Catalyst operation mode and regeneration

The applicability of the SDR with coated TiO_2 was confirmed, since up to 10 disc regeneration cycles were performed without loss in efficiency (Figure 9), confirming that the SDR is an interesting alternative to traditional reactor configurations, avoiding TiO_2 filtration. Thermal regeneration was performed by calcination each time after the experiment at 500 ºC for 2 hours.

Figure 9

4. CONCLUSIONS

- The photo-degradation process of AP was studied in a novel spinning disc reactor (SDR) under a heterogeneous process (UV-H_2O_2/TiO_2). The synergism between the individual processes and the overall UV/H_2O_2/TiO_2 system was quantified to be 47%.

- A factorial design of experiments followed by a Neural Networks fitting allowed to obtain the optimal conditions: pH= 4; [H_2O_2]0= 1500 mg/L; disc speed= 500 rpm; flowrate = 25 mL/s. Under these conditions, 50 mg/L of AP were completely degraded in 120 minutes. The process can be made after disc regeneration up to 10 cycles with no loss in efficiency. This is the first comprehensive mapping out the effect of the important operating parameters of the photocatalytic spinning disc reactor, by applying statistical experimental design. As this has not been done for SDRs in general, this is therefore the first comprehensive assessment of the operating space for this important class of process intensification reactor.

- There is no apparent decrease in the order of magnitude of reaction rate (the apparent volumetric rate constant ranges from $2.05 \bullet 10^{-4}$ to $4.82 \bullet 10^{-4}$ s^{-1}) with film height (111-222 μm) as estimated with the approximate Nusselt model. There is no dependence of the photonic efficiency on the film height either, so it is reasonable to believe that no mass transfer limitations are occurring.

- After intermediates identification, a simple mechanism can be proposed for AP photodegradation during the $UV/H_2O_2/TiO_2$ process. Anthranilic acid, 1,4-benzenedicarboxylic acid and benzenamide would be the main reaction intermediates. The phenyl ring of all of them would be later opened to form small molecular organic acids (2-butenedioic acid, butenedioic acid and 4-oxopentanoic acid).

- Given the above mechanism and optimized reaction conditions determined, this work shows that the phocatalytic SDR is an effective and robust wastewater treatment technology for the degradation of antipyrine producing degradation products (such as molecular organic acids) that could be further mineralised by conventional biological wastewater treatment systems.

5. ACKNOWLEDGEMENTS

Financial support from MINECO (CTM2013-44317-R) and from UCLM (Ayuda para la Financiación de Grupos de Investigación GI20142907) is gratefully acknowledged.

476 The authors also acknowledge financial support from Marie Curie Career Integration
477 Grant (CIG) FP7- 333952 and from the University of Bath International Research Fund
478 Future Research Leaders Incubator Scheme.

479 The authors would also like to thank Fernando Ramon Acosta, Daniel Lou-Hing,
480 Alexander Ciupa and Anneke Lubben at the University of Bath for technical support in
481 this work.

482

483 NOMENCLATURE

484 v kinematic viscosity ($m^2\ s^{-1}$)

485 ω rotational speed of spinning disc (rad s^{-1})

486 Q volumetric flow rate ($m^3\ s^{-1}$)

487 h height of the liquid film at radius r (m)

488 R_i reaction rate (mol/L s)

489 C concentration of substrate (mol/L)

490 C_0 initial concentration of substrate (mol/L)

491 V reactor volume (m^3)

492 k_{app} pseudo-first or second order reaction rate constant based on reactor volume (s^{-1})

493 A Nusselt film height equation constant ($m^{5/3}$)

494 R outer disc radius (m)

495 R_0 inlet nozzle radius (m)

496 t time (s)

497

498

6. REFERENCES

Boiarkina, I, Norris, S., Patterson, D. A., 2013. Investigation into the effect of flow structure on the photocatalytic degradation of methylene blue and dehydroabietic acid in a spinning disc reactor, Chem. Eng. J. 222, 159-171.

Boiarkina, I, Pedron, S., Patterson, D. A., 2011. An experimental and modelling investigation of the effect of the flow regime on the photocatalytic degradation of methylene blue on a thin film coated ultraviolet irradiated spinning disc reactor, Appl. Catal. B: Environ., 110, 14-24.

Boodhoo, K. V. K., Jachuck, R.J., 2000. Process intensification: spinning disk reactor for styrene polymerisation, Appl. Thermal Eng., 20, 1127-1146.

Burns, J.R., Ramshaw, C., Jachuck, R.J., 2003. Measurement of liquid film thickness and the determination of spin-up radius on a rotating disc using an electrical resistance technique, Chem. Engi. Sci., 58 (11), 2245–2253.

Cai, M., Zhang, L., Qi, F., Feng, L., 2013. Influencing factors and degradation products of antipyrine chlorination in water with free chlorine. J. Environ. Sci., 25(1), 77-84.

Caprariis, B., Di Rita, M., Stoller, M., Verdone, N., Chianese, A., 2012. Reaction-precipitation by a spinning disc reactor: influence of hydrodynamics on nanoparticles production. Chem. Eng. J. 76, 73-80.

Daneshvar, N., Rabbani, M., Modirshahla, N. and Behnajady, M.A., 2004. Kinetic modelling of photocatalytic degradation of Acid Red 27 in UV/TiO_2 process. J. Photochem. Photobiol. A: Chem. 168, 39-45.

Domínguez Sánchez, L., Michel Taxt-Lamolle, S. F., Olaug Hole, E., Krivokapic, A., Sagstuen, E., Jostein Haugen, H., 2013. TiO_2 suspension exposed to H_2O_2 in ambient light

523 or darkness: Degradation of methylene blue and EPR evidence for radical oxygen species,
524 Appl. Catal. B: Environ., 142-143, 662-667.
525 Domínguez, S., Ribao, P., Rivero, M. J., Ortiz, I. 2015. Influence of radiation and TiO_2
526 concentration on the hydroxyl radicals generation in a photocatalytic LED reactor.
527 Application to dodecylbenzenesulfonate degradation, Appl. Catal. B: Environ., 178, 165-
528 169.
529 Durán, A., Monteagudo, J. M., Sanmartín, I., García-Díaz, A. 2013. Sonophotocatalytic
530 mineralization of antipyrine in aqueous solution, Appl. Catal. B: Environ., 138-139, 318-
531 325.
532 Durán, A., Monteagudo, J.M., Sanmartín, I., García-Díaz, A., 2013. Sonophotocatalytic
533 mineralization of antipyrine in aqueous solution. Appl. Catal. B: Environ. 138–139, 318–
534 325.
535 Galindo, C., Jacques, P. and Kalt, A., 2001. Photooxidation of the phenylazonaphthol
536 AO20 on TiO_2: kinetic and mechanistic investigations. Chemosphere 45, 997-1005.
537 Joseph, C.G., Li Puma, G., Bono, A., Taufiq-Yap, Y.H., Krishnaiah, D. 2011. Operating
538 parameters and synergistic effects of combining ultrasound and ultraviolet irradiation in
539 the degradation of 2,4,6-trichlorophenol, Desalination 276, 303-309.

540 Khatae, A.R., Kasiri, M.B., 2010. Artificial neural networks modeling of contaminated
541 water treatment processes by homogeneous and heterogeneous nanocatalysis., J. Molec.
542 Catal. A: Chem. 331, 86-100

543 Li, X., Cao, R., Lin, Q., Solvent-free Baeyer–Villiger oxidation with H_2O_2 as oxidant
544 catalyzed by multi-SO_3H functionalized heteropolyanion-based ionic hybrids, Catal.
545 Commun. 63, 79-83.

546 Li, X., Chen, C., Zhao J., 2001. Mechanism of photodecomposition of H_2O_2 on TiO_2
547 surfaces under visible light irradiation, Langmuir, 17, 4118-4122.
548 Ling, C.M., Mohamed, A.R., Bhatia, S., 2004. Performance of photocatalytic reactors
549 using immobilized TiO_2 film for the degradation of phenol and methylene blue dye
550 present in water stream, Chemosphere, 57, 547-554.
551 Liu, Y., He, X., Fu, Y., Dionysiou, D. D., 2016. Degradation kinetics and mechanism of
552 oxytetracycline by hydroxyl radical-based advanced oxidation processes, Chem. Eng. J.,
553 284, 1317-1327.
554 Matta, R., Tlili, S., Chiron, S., Barbati, S., 2011, Removal of carbamazepine from urban
555 wastewater by sulfate radical oxidation, Environ. Chem. Lett., 9, 347–353.
556 Miao, H.F., Cao, M., Ren, H.Y., Zhao, M.X., Huang, Z.X., Ruan, W.Q., 2015.
557 Degradation of phenazone in aqueous solution with ozone : influencing factors and
558 degradation pathways. Chemosphere 119, 326-333.
559 Miralles-Cuevas, S., Prieto-Rodríguez, L., Torres-Socías, E., Polo-López, M.I.,
560 Fernández-Ibáñez, P., Oller, I., Malato, S., 2014. Strategies for hydrogen peroxide dosing
561 based on dissolved oxygen concetration for solar photo-Fenton treatment of complex
562 wastewater, Global Nest J. 16, 553-560.
563 Miranda-García, N., Suárez, S., Ignacio Maldonado, M., Malato, S., Sánchez, B., 2014.
564 Regeneration approaches for TiO_2 immobilized photocatalyst used in the elimination of
565 emerging contaminants in water, Catal. Today, 230, 27-34.
566 Molinari, R., Pirillo, F., Loddo, V., Palmisano, P., 2006., Heterogeneous photocatalytic
567 degradation of pharmaceuticals in water by using polycrystalline TiO_2 and a
568 nanofiltration membrane reactor. Catal. Today 118, 205-213.

569 Monteagudo, J.M., Durán, A., Guerra, J., García-Peña, F., Coca, P., 2008. Solar TiO_2-
570 assisted photocatalytic degradation of IGCC power station effluents using a Fresnel lens,
571 Chemosphere, 71, 161-167.
572 Monteagudo, J.M., Durán, A., López-Almodóvar, 2008. Homogeneous ferrioxalate-
573 assisted solar photo-Fenton degradation of Orange II aqueous solution, Appl.
574 Catal.B:Environ 83, 46-55.
575 Morgan, D.P. and Scofield, C.L., 1991. Neural Networks and Speech Processing.
576 Kluwver Academic Publishers. London.
577 Naeem. K., Ouyang, F. 2013. Influence of supports on photocatalytic degradation of
578 phenol and 4-chlorophenol in aqueous suspensions of titanium dioxide, J. Environ. Sci.
579 25, 399-404.
580 Nath, R., Rajagopalan, B., Ryker, R., 1997. Determining the saliency of input neural
581 classifiers, Comput. Oper. Res., 24, 767-773.
582 Rao, Y. F., Chu, W., 2009. Reaction Mechanism of Linuron Degradation in TiO_2
583 Suspension under Visible Light Irradiation with the Assistance of H_2O_2. Environ. Sci.
584 Technol. 43, 6183-6189.
585 Tana, C., Gaoa, N., Dengb, Y., Zhanga, Y., Suia, M., Denga, J., Zhoua, S., 2013.
586 Degradation of antipyrine by UV, UV/H_2O_2 and UV/PS. J. Hazar. Mater. 260, 1008–
587 1016.
588 Verlichi, P., Al Aukidy, M., Zambello, E., 2012. Occurrence of pharmaceutical
589 compounds in urban wastewater: removal, mass loa and environmental risk after a
590 secondary treatment-a review. Sci. Total Environ. 429, 123-155.
591
592
593
594

595 **FIGURE CAPTIONS**

596 **Figure 1.** Experimental installation. a) schematic diagram, b) reactor, c) detail of the
597 scanning disc.

598 **Figure 2.** Antipyrine removal (%) under different systems. $[AP]_0$= 35 mg/L; $[H_2O_2]_0$=
599 1000 mg/L; Speed= 300 rpm; Flow= 15 mL/s.

600 **Figure 3.** Effect of variables in antipyrine degradation for the UV/H_2O_2/TiO_2 process.
601 Simulation from neural networks at the central point. a) $[H_2O_2]_0$ vs pH (Flow= 15 mL/s,
602 Speed = 300 rpm), b) Speed vs Flow ($[H_2O_2]_0$ = 1000 mg/L; pH = 6).

603 **Figure 4**. Distribution of film thickness on the disc according to Eq (5) under optimal
604 conditions.

605 **Figure 5.** Results under optimal conditions (pH= 4; $[H_2O_2]_0$= 1500 mg/L; Speed= 500
606 rpm; Flow= 25 mL/s; $[AP]_0$= 50 mg/L) a) [AP] and $[H_2O_2]$; b) TOC concentration.

607 **Figure 6.** Influence of a) temperature and b) dissolved O_2 concentration under optimal
608 conditions (pH= 4; $[H_2O_2]_0$= 1500 mg/L; Speed= 500 rpm; Flow= 25 mL/s; $[AP]_0$= 50
609 mg/L).

610 **Figure 7.** Intermediates evolution obtained by MS (Conditions: pH= 4; $[H_2O_2]0$= 1500
611 mg/L; Speed= 500 rpm; Flow= 25 mL/s; $[AP]_0$= 50 mg/L).

612 **Figure 8.** Antypirine degradation pathway induced by UV/H_2O_2/TiO_2 (adapted from
613 [28])

614 **Figure 9.** Catalysis behavior after regeneration under optimal conditions (pH= 4;
615 $[H_2O_2]_0$= 1500 mg/L; Speed= 500 rpm; Flow= 25 mL/s; $[AP]_0$= 50 mg/L)

616

617

618

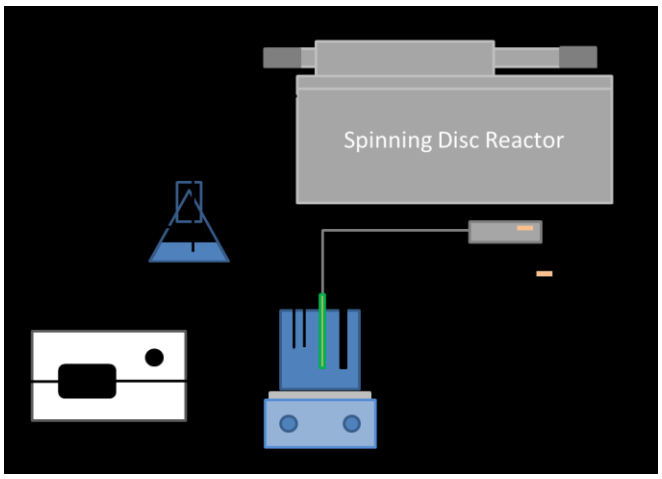
Spinning Disc Reactor

a)

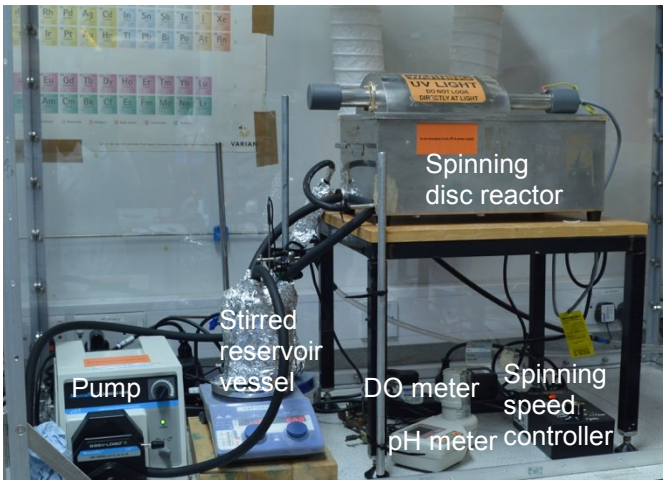
Spinning
disc reactor
Stirred
reservoir
vessel
Pump
DO meter
Spinning
speed
controller
pH meter

b)

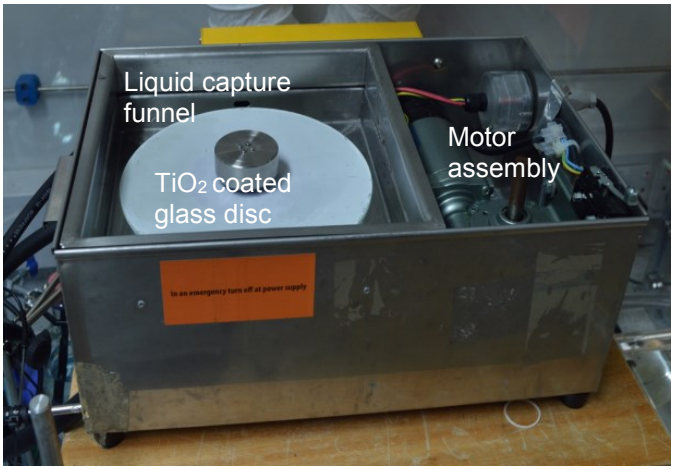
Liquid capture
funnel
Motor
assembly
TiO2 coated
glass disc

c)

FIGURE 1

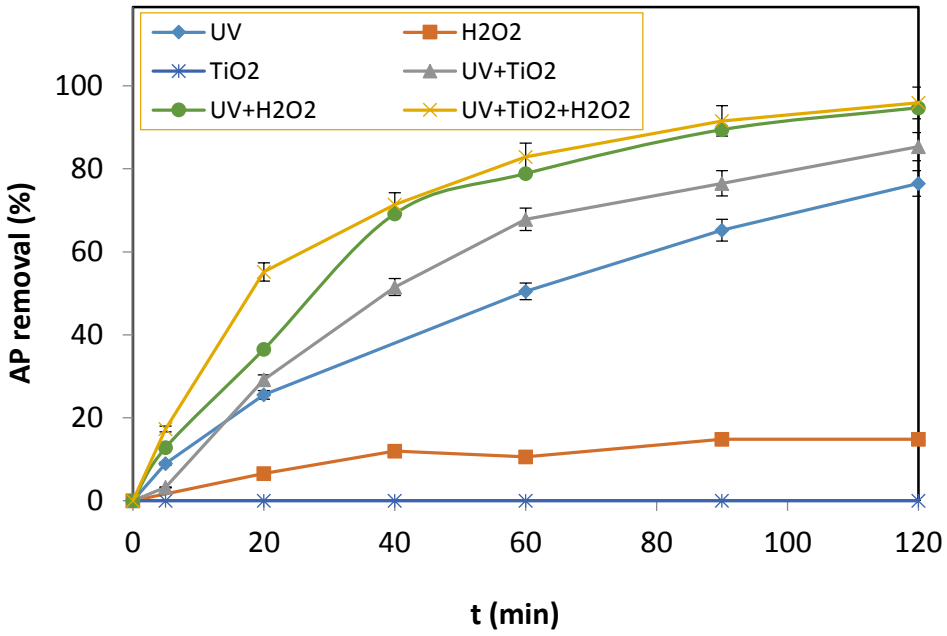
UV
H2O2
TiO2
UV+TiO2
UV+H2O2
UV+TiO2+H2O2
AP removal (%)
0
20
40
60
80
100
0
20
40
60
80
100
120
t (min)

FIGURE 2

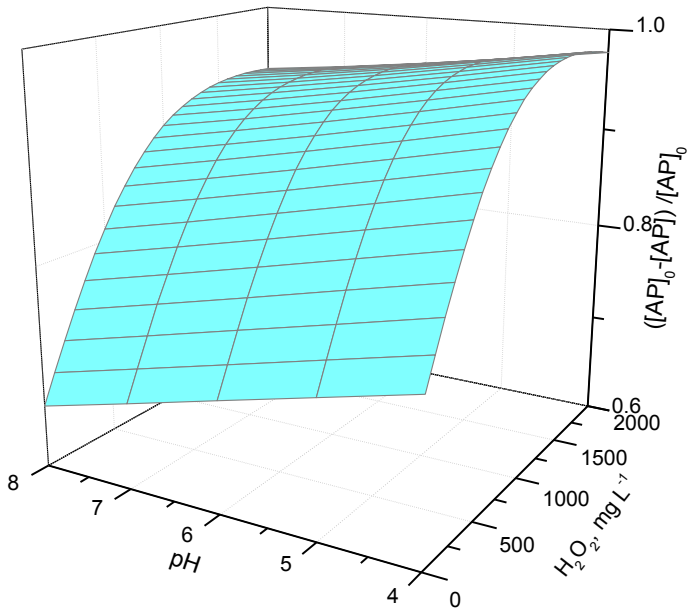
1.0
0.8
0.6
([AP]0-[AP]) /[AP]0
8
7
6
5
4
pH
0
500
1000
1500
2000
H2O2, mg L-1

a)

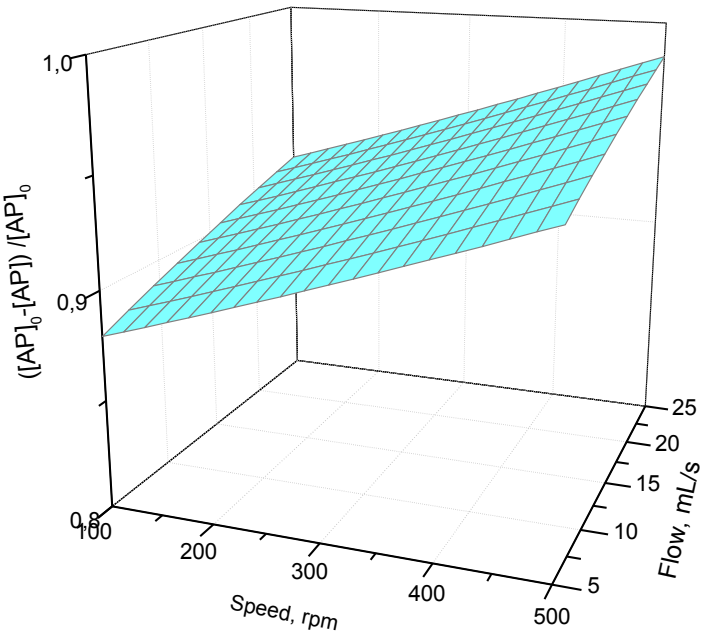
1,0
0,9
0,8
([AP]0-[AP]) /[AP]0
100
200
300
400
500
Speed, rpm
5
10
15
20
25
Flow, mL/s

b)

FIGURE

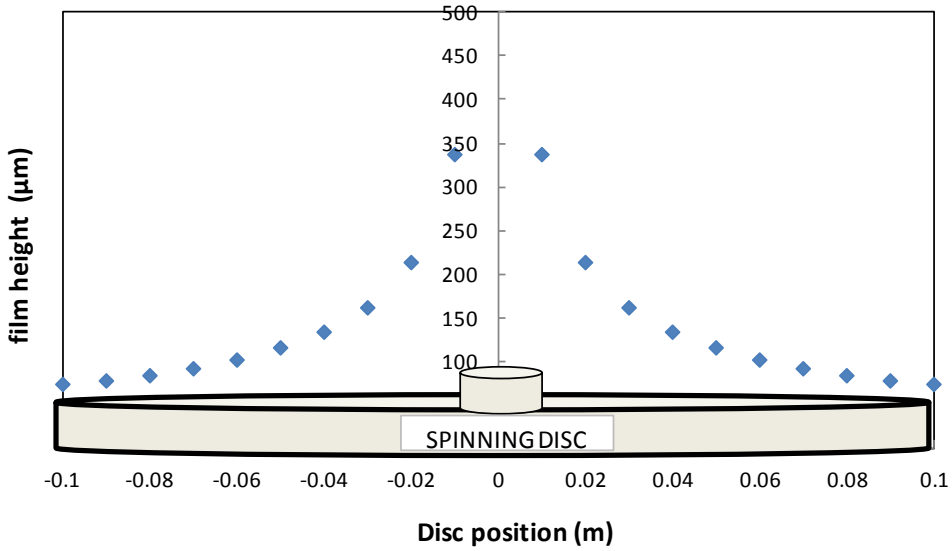
film height (µm)
500
450
400
350
300
250
200
150
100
SPINNING DISC
-0.1
-0.08
-0.06
-0.04
-0.02
0
0.02
0.04
0.06
0.08
0.1
Disc position (m)

FIGURE 4

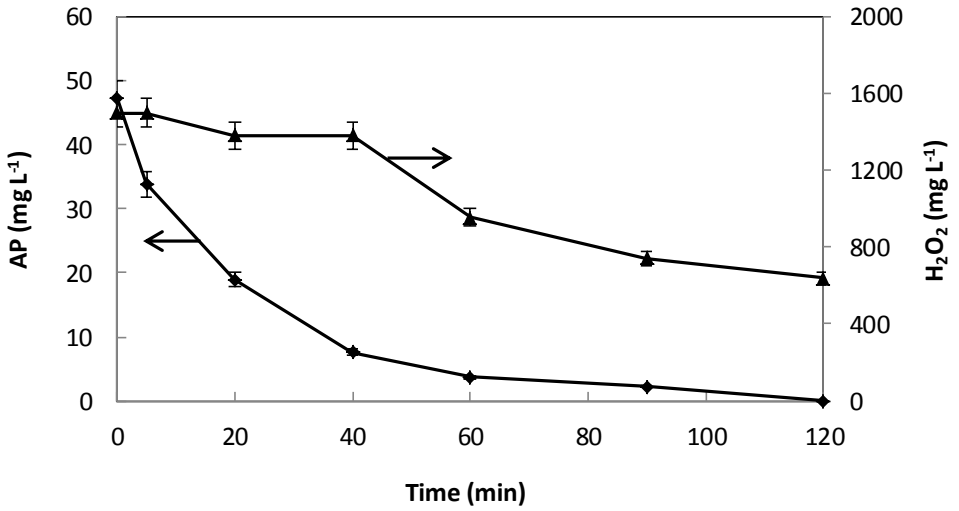
AP (mg L-1)
H2O2 (mg L-1)
Time (min)
0
10
20
30
40
50
60
0
400
800
1200
1600
2000
0
20
40
60
80
100
120

a)

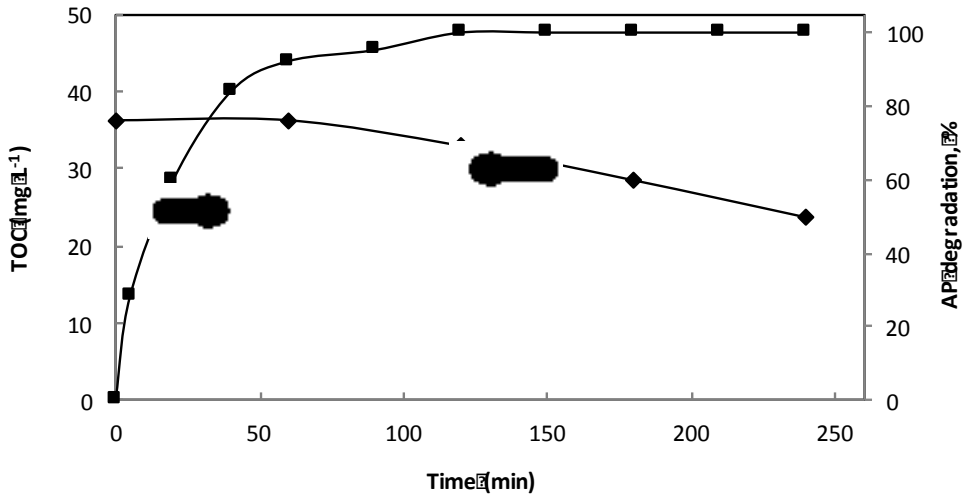
TOC (mg L-1)
AP degradation, %
Time (min)
0
10
20
30
40
50
0
20
40
60
80
100
0
50
100
150
200
250

b)

FIGURE 5

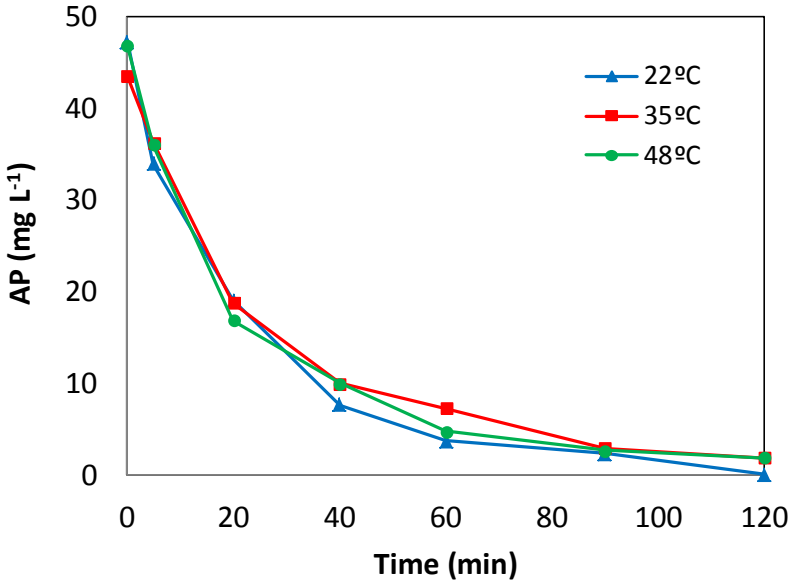
50
40
30
20
10
0
AP (mg L-1)
0
20
40
60
80
100
120
Time (min)
22ºC
35ºC
48ºC

a)

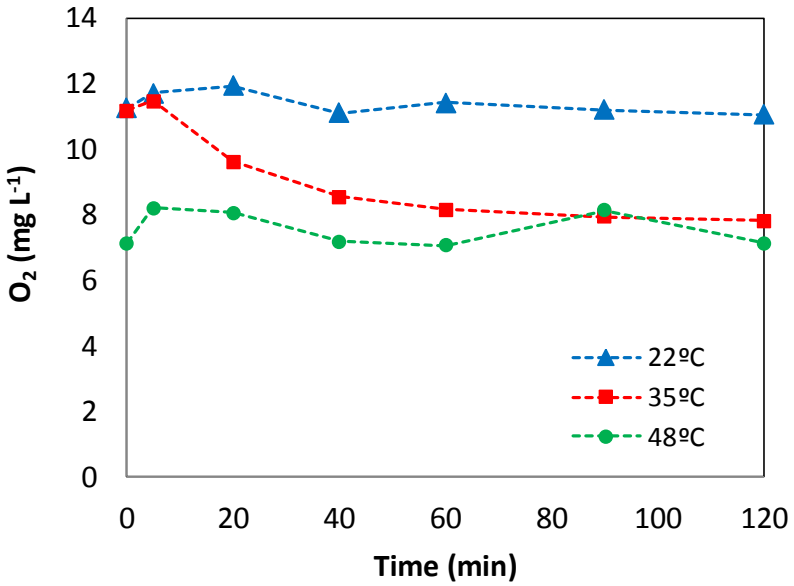
14
12
10
8
6
4
2
0
O2 (mg L-1)
0
20
40
60
80
100
120
Time (min)
22ºC
35ºC
48ºC

b)

FIGURE 6

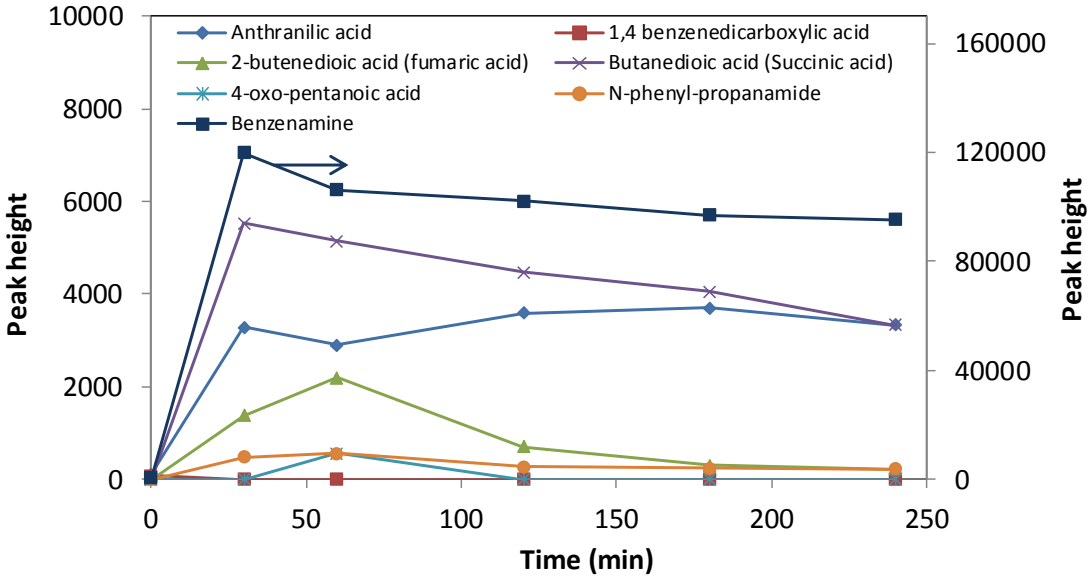
Anthranilic acid
1,4 benzenedicarboxylic acid
2-butenedioic acid (fumaric acid)
Butanedioic acid (Succinic acid)
4-oxo-pentanoic acid
N-phenyl-propanamide
Benzenamine
Peak height
Peak height
Time (min)
0
2000
4000
6000
8000
10000
0
40000
80000
120000
160000
0
50
100
150
200
250

FIGURE 7

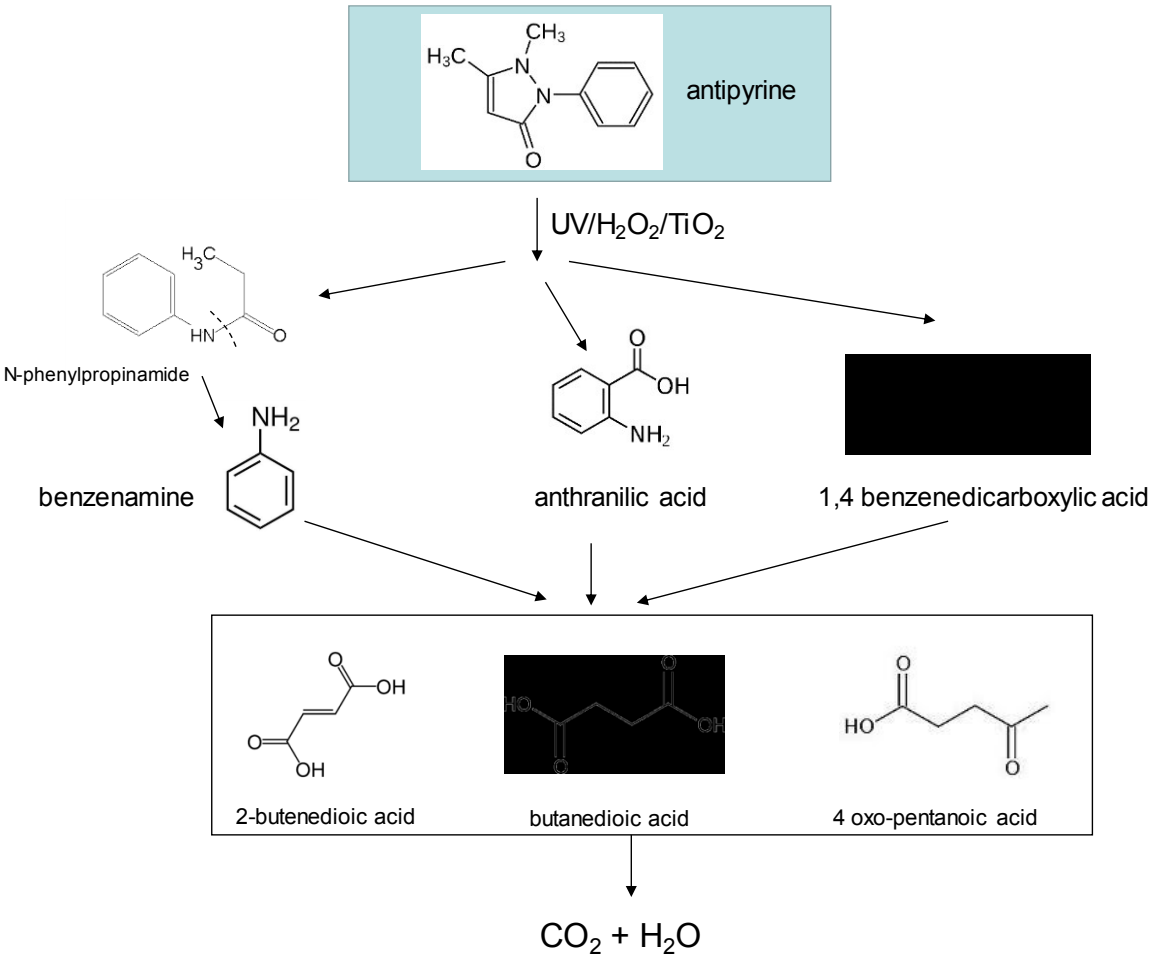
antipyrine
UV/H2O2/TiO2
N-phenylpropinamide
benzenamine
anthranilic acid
1,4 benzenedicarboxylic acid
2-butenedioic acid
butanedioic acid
4 oxo-pentanoic acid
CO2 + H2O

FIGURE 8

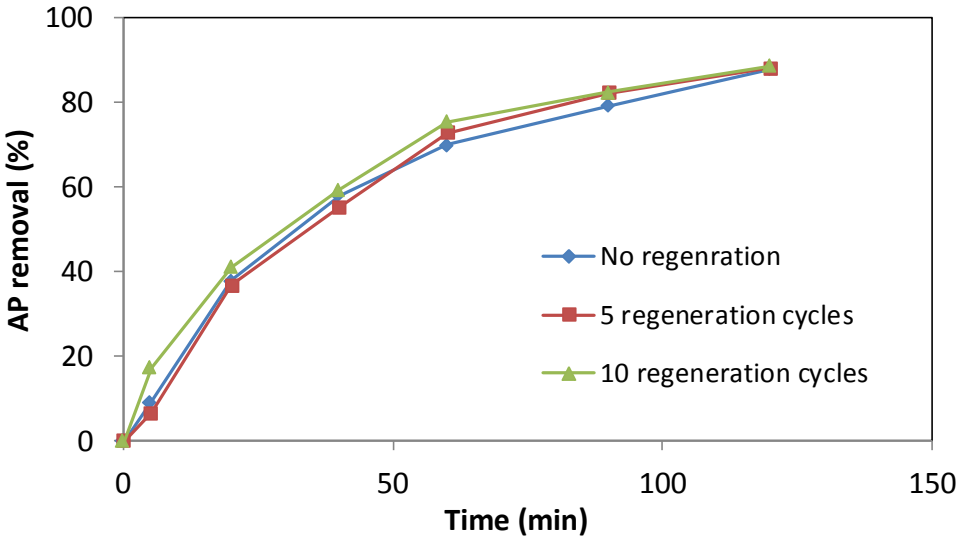
100
80
60
40
20
0
AP removal (%)
0
50
100
150
Time (min)
No regenration
5 regeneration cycles
10 regeneration cycles

FIGURE 9

SUPPLEMENTARY MATERIAL

Table 1. Experimental design, film thickness and apparent volumetric rate constant for the degradation of antipyrine in SDR.

Process: UV/H_2O_2/TiO_2

Factorial Design					Response Function after 120 minutes		
Experiment	**H_2O_2 (mg/L)**	**Speed (rpm)**	**Flow (mL/s)**	**pH**	**$([AP]_0-[AP])/[AP]_0$**	**k *10^4 (s^{-1})**	**h (µm)**
1	1125	400	20	7	0,981	4.848	
2	375	400	20	7	0,827	3.322	138.1
3	1125	400	20	5	0,984	5.180	
4	375	400	20	5	0,879	2.930	
5	1125	400	10	7	0,926	3.607	
6	375	400	10	7	0,812	2.523	111.0
7	1125	400	10	5	0,956	4.384	
8	375	400	10	5	0,865	2.694	
9	1125	200	20	7	0,918	3.352	
10	375	200	20	7	0,824	2.323	
11	1125	200	20	5	0,938	3.838	222.0
12	375	200	20	5	0,849	2.657	
13	1125	200	10	7	0,918	3.362	
14	375	200	10	7	0,759	2.055	176.2
15	1125	200	10	5	0,937	3.670	
16	375	200	10	5	0,780	2.118	
17	1500	300	15	6	0,985	4.297	
18	0	300	15	6	0,709	1.689	153.9
19	750	300	15	8	0,856	3.320	
20	750	300	15	4	0,943	3.938	
21	750	300	25	6	0,917	3.503	182.5
22	750	300	5	6	0,872	3.007	106.7
23	750	500	15	6	0,940	3.770	109.4
24	750	100	15	6	0,868	2.850	320.3
25	750	300	15	6	0,904	3.460	
26	750	300	15	6	0,879	2.888	
27	750	300	15	6	0,880	3.027	153.9
28	750	300	15	6	0,886	2.887	
Additional Experiments (for determination of optimum conditions)							
29	1750	300	15	6	0,956	4.372	153.9
30	2000	300	15	6	0,951	4.389	

847
848 **Table 2. Equation and parameters for the NN fitting.**
849 **(Process: UV/H_2O_2/TiO_2)**
850

$$\frac{[AP]_0 - [AP]}{[AP]_0} = N_1 \cdot \left(1 + \frac{1}{e^{(W_{11}\cdot[H_2O_2]_0 + W_{12}\cdot Speed + W_{13}\cdot Flow + W_{14}\cdot pH)}}\right) + N_2 \cdot \left(1 + \frac{1}{e^{(W_{21}\cdot[H_2O_2]_0 + W_{22}\cdot Speed + W_{23}\cdot Flow + W_{24}\cdot pH)}}\right)$$

Neurons and Weight Factors	Parameters	Values of neurons and factors
N_1	**Neuron**	0.88
W_{11}	$[H_2O_2]_0$	3.81
W_{12}	Speed	0.11
W_{13}	Flow	0.43
W_{14}	pH	-0.1
N_2	**Neuron**	0.44
W_{21}	$[H_2O_2]_0$	-1.44
W_{22}	Speed	0.59
W_{23}	Flow	0.01
W_{24}	pH	-0.66

851
852
853
854
855
856
857
858
859
860
861
862
863

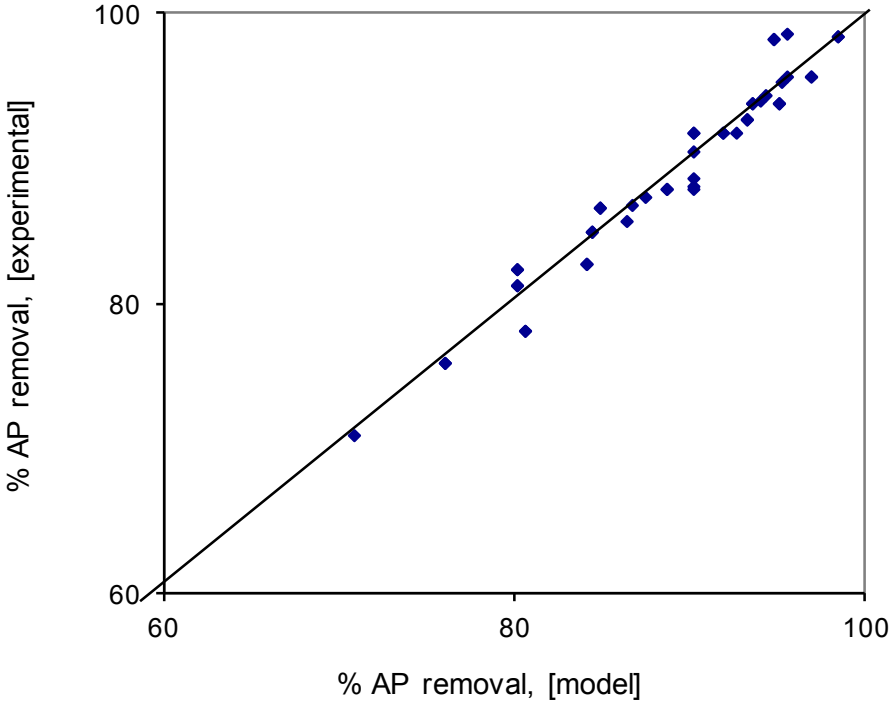

Figure S1. Neural network fitting for the UV/H_2O_2/TiO_2 system

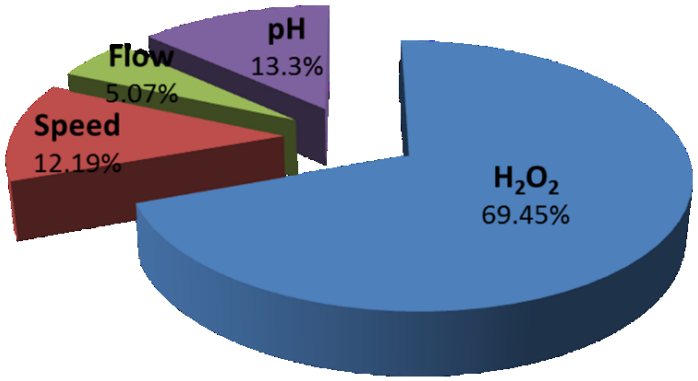

Figure S2. Saliency Analysis for the UV/H_2O_2/TiO_2 system (%).

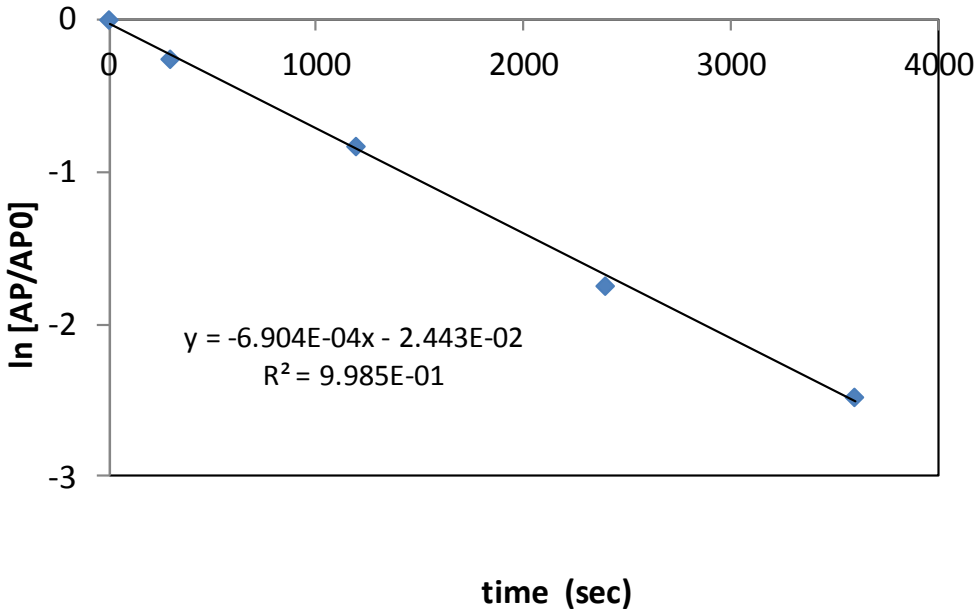

Figure S3. Example of fitting of the reaction order for the UV/H_2O_2/TiO_2 system Conditions: pH= 4; $[H_2O_2]_0$= 1500 mg/L; Speed= 500 rpm; Flow= 25 mL/s; $[AP]_0$= 50 mg/L.

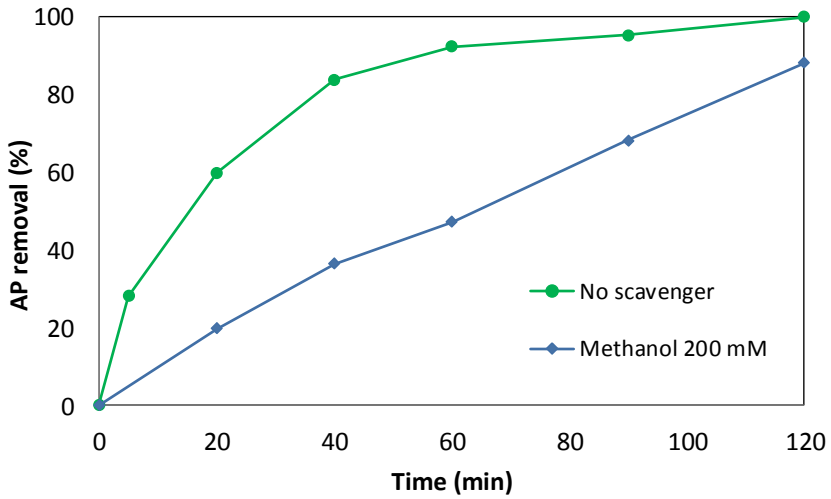

Figure S4. Scavenger effect (effect of methanol addition to the UV/H_2O_2/TiO_2 system). Conditions: pH= 4; $[H_2O_2]_0$= 1500 mg/L; Speed= 500 rpm; Flow= 25 mL/s; $[AP]_0$= 50 mg/L.